Title
X-ray-absorption studies of cation ordering and valence in the T*-phase La2-x-yRxSryCuO4 (R=Sm, Eu, Gd, Tb, and Dy)

Journal
Physical Review B, 44(13)

ISSN
2469-9950

Authors
Tan, Zhengquan
Budnick, JI
Luo, Sheng
et al.

Publication Date
1991-10-01

DOI
10.1103/physrevb.44.7008

X-ray-absorption studies of cation ordering and valence in the T^*-phase $La_{2-x-y}R_xSr_yCuO_4$ (R = Sm, Eu, Gd, Tb, and Dy)

Zhengquan Tan,* J. I. Budnick, Sheng Luo, and W. Q. Chen
Physics Department and Institute of Materials Science, The University of Connecticut, Storrs, Connecticut 06269-3046

S-W. Cheong and A. S. Cooper
AT&T Bell Laboratories, Murray Hill, New Jersey 07974-2070

P. C. Canfield and Z. Fisk
Los Alamos National Laboratory, Los Alamos, New Mexico 87545
(Received 25 February 1991; revised manuscript received 30 April 1991)

X-ray-absorption measurements have been made at the lanthanide L edges, Sr and Cu K edges in the T^*-phase $La_{2-x-y}R_xSr_yCuO_4$ compounds with R=Sm, Eu, Gd, Tb, and Dy. The La and rare-earth x-ray-absorption near-edge (XANES) data and the extended x-ray-absorption fine-structure data both clearly indicate that the R and La ions selectively enter the M' site and M site, respectively. The degree of this site ordering is nearly perfect and is similar for the Sm, Eu, Gd, Tb, and Dy members of this family. The L_3 XANES data show that the La, Sm, Eu, Gd, and Dy are trivalent in these compounds, but about 20% of the Tb ions are tetravalent in the Tb material. The Cu K-edge XANES spectra are consistent with a divalent state for copper, and are essentially identical for the as-prepared nonsuperconducting samples and the high-pressure oxygenated superconducting counterparts. This indirectly suggests that the hole carrier in the T^*-phase superconductors is largely associated with oxygen atoms as in $La_{1.85}Sr_{0.15}CuO_4$. Based on the results of cation-ordering, cation-valence, and oxygen-content measurements, the superconducting behavior of Sm, Em, and Gd T^* phases and the lack of superconductivity in the Tb and Dy compounds are discussed.

I. INTRODUCTION

The T^*-phase compounds $(Nd,Ce,Sr)_2CuO_4$ (Refs. 1–3) and $La_{2-x-y}R_xSr_yCuO_4$, with R=Sm, Eu, and Gd,[4–6] exhibit superconductivity with transition temperatures (T_c) above 30 K. This provides a channel for studying the mechanism(s) of high-T_c superconductivity, especially considering the relationship between the T^* materials and T-phase $La_{2-x}Sr_xCuO_4$ and T'-phase $Nd_{2-x}Ce_xCuO_4$ superconductors. The T^* phases themselves possess many interesting properties which distinguish them from other materials. For example, high-pressure oxygen treatment is necessary for producing superconductivity in $La_{2-x-y}R_xSr_yCuO_4$ (R=Sm, Eu, and Gd) and, to a lesser degree, in $(Nd,Ce,Sr)_2CuO_4$. The values of T_c depend strongly on the conditions of oxygenation. The T^* structure forms with a combination of a variety of large and smaller lanthanides, but the phase homogeneity range appears to be rather narrow.

The T^* structure is closely related to the K_2NiF_4-type (T) and Nd_2CuO_4-type (T') structures in that its unit cell consists of half of the T and half of the T' unit cells stacked along the tetragonal c axis.[7] There are two inequivalent lanthanide sites in the T^* structure; the M site is locally similar to the La site in La_2CuO_4, and the M' site is locally similar to the Nd site in Nd_2CuO_4. Based on neutron-diffraction data, Izumi *et al.*[8] suggested that Sr and Ce preferentially enter the M and M' sites respectively in the $(Nd,Ce,Sr)_2CuO_4$ system. Kwei *et al.*[9] have found in $La_{0.9}Gd_{0.9}Sr_{0.2}CuO_4$ that Gd enters only the M' site and Sr and La occupy the M site and remaining M' positions. Our x-ray absorption data have shown that the lanthanide cations are ordered in $La_{0.9}R_{0.9}Sr_{0.2}CuO_4$ for R=Sm, Eu, Gd, and Tb.[10] Site ordering between La and Dy ions in $La_{1.25}Dy_{0.75}CuO_4$ has also been observed.[11] The cation site ordering in the T^* structure appears to be a general characteristic and closely related to the ionic radii disparity. What remains unclear is whether the degree of site ordering varies with different cation combinations and how it affects the physical properties of the material. We have thus attempted to determine the local environment of La and rare-earth ions in the T^* phases $La_{0.9}R_{0.9}Sr_{0.2}CuO_4$ with R=Sm, Eu, Gd, Tb, and Dy, by studying the x-ray-absorption spectra near the L_3 edge of each element. Both x-ray-absorption near-edge structure (XANES) and extended x-ray-absorption fine structure (EXAFS) data indicate that La and R ions are nearly perfectly ordered with the smaller R ions occupying only the M' site and the larger Sr and La occupying the M site and the rest of the M' sites. Within our experimental uncertainty, the degree of cation site ordering is similar for rare earths from Sm through Dy.

In the T^*-phase $La_{2-x-y}R_xSr_yCuO_4$ family, the Sm, Eu, and Gd members become superconducting after high-pressure oxygen treatment. However, the Tb and Dy members are not superconducting under similar treatment.[6] If we assume that the rare earths in these materials are trivalent, then Sr^{2+} seems to play the role of a

hole dopant. The need of oxygen treatment for producing metalliclike conductivity and superconductivity suggest that oxygen vacancies may exist in the untreated materials. The oxygen vacancies in Tb and Dy phases could persist even after high-pressure oxygenation. In the case of Tb T^* compounds, another possibility is that some tetravalent Tb may be present and compensates the hole doped by Sr. A direct determination of the rare-earth valence is needed to resolve these possibilities. Our L_3 XANES data indeed indicate that a significant amount of Tb in the T^* phase is tetravalent, while La, Sm, Eu, Gd, and Dy assume only a trivalent state.

While charge carriers are holes in the T-phase $La_{2-x}Sr_xCuO_4$ and electrons in the T'-phase $Nd_{2-x}Ce_xCuO_4$ superconductors, Hall-coefficient measurements[3] and the behavior of conductivity with oxygen treatment[2,3,5] suggest that the carriers in the T^* superconductors are holes. Attempts to introduce n-type carriers have not been able to produce superconductivity in the T^* structure.[12–14] The ability to accept holes or electrons in the CuO_2 planes appears to be related to the oxygen coordination configuration around the copper ion. In addition to four oxygens in the plane common to the T, T^*, and T' structures, the copper is further coordinated with two apical (out-of-plane) oxygens in the T compounds and one apical oxygen in the T^* compounds. We report the Cu K-edge XANES data and discuss the local electronic properties and their relation to doping.

II. EXPERIMENTS

Polycrystalline samples were prepared by firing appropriate mixtures of starting materials in the form of powders and pellets in air. High-purity metal oxides L_2O_3 (L=La, Sm, Eu, Gd, and Dy), Tb_4O_7, CuO, and $SrCO_3$ were used for starting materials. In particular, T^*-phase $La_{0.9}R_{0.9}Sr_{0.2}CuO_4$ were prepared as described previously.[4] We will denote the air-fired samples as "as-prepared" and label the individual $La_{0.9}R_{0.9}Sr_{0.2}CuO_4$ samples as $R_{0.9}$ for brevity; for example, $Sm_{0.9}$ stands for the $La_{0.9}Sm_{0.9}CuO_4$ sample. The as-prepared T^*-phase samples showed no superconductivity down to 5 K. As reported previously,[4–6] the Sm, Eu, and Gd members become superconducting after high-pressure oxygen annealing. In the present experiments, we have treated the $Sm_{0.9}$, $Tb_{0.9}$, and $Dy_{0.9}$ samples in 160 bars of oxygen at 575°C for at lease 18 h. The Sm sample is superconducting with an onset of diamagnetism at 21 K, but the Tb and Dy analogs are not superconducting. The x-ray-absorption results presented below are for the as-prepared samples unless otherwise noted.

For reference purposes, samples of T-phase $La_{1.85}Sr_{0.15}CuO_4$, $La_{1.4}Sm_{0.4}Sr_{0.2}CuO_4$, T'-phase R_2CuO_4 (R=Nd, Sm, Eu, and Gd), and Nd_2CuO_4 with La, Tb, and Dy substituting for part of Nd were also prepared. All samples were characterized by x-ray powder diffraction to check the phase purity. The $La_{1.4}Sm_{0.4}Sr_{0.2}CuO_4$ is dominantly T phase with about 5% T^*-phase impurity. Other samples are single phase. The $Nd_{1.8}Tb_{0.2}CuO_4$ and $Nd_{1.8}Dy_{0.2}CuO_4$ samples showed a clear decrease in the c-axis lattice constant as compared to Nd_2CuO_4, as expected.

X-ray-absorption experiments were carried out at the National Synchrotron Light Source (NSLS) on Beam Line X-11A using a Si(111) double-crystal monochromator. For La and rare-earth L edges, the monochromator entrance-slit vertical separation was set at 0.5 mm and both XANES and EXAFS were measured in a single scan. The Cu K-edge XANES and EXAFS spectra were taken separately using a 0.25 and 0.50-mm slit, respectively. Usually, a reference spectrum was simultaneously measured in a second channel along with the sample for energy calibration. Samples were made in the form of four to six layers of fine powders rubbed on Scotch tape. The spectra were obtained in the transmission mode for concentrated absorbers and in the fluorescence mode for diluted absorbers using gas-ionzation chambers as detectors. We note that in transmission measurements of samples in the present form the intensity of the strong L_3 main peak (white line) may be slightly reduced because of a thickness effect, while other spectral features are not affected. Fortunately, none of our results relies on an accurate measurement of the white-line intensity.

III. CATION SITE ORDERING

A. Lanthanide XANES results

In this section we use the La and rare-earth L_3 XANES spectra to determine the valence state and site location of these ions in the T^* compounds $La_{2-x-y}R_xSr_yCuO_4$. The site location is inferred from a comparison of the spectra of T^* samples to those of T and T' compounds in which there is only one La or rare-earth site. This is made possible by the identification of a unique spectral feature. The site location is also determined independently by the analysis of the L_3 EXAFS data, which will be presented in the next section.

The XANES spectra presented here are normalized to the edge jump after the preedge background subtraction. The energy reference E_0 for the L_3 edge was chosen at the half-height point of the absorption edge, since this choice gave the most reproducible energy scale for the EXAFS data. Figure 1(a) presents the L_3 XANES data of La and rare earths in the T^* compounds $La_{0.9}R_{0.9}Sr_{0.2}CuO_4$ and in trivalent lanthanide oxides. The edge position is sensitive to the valence state of the absorbing atom. In general, the edge shifts to a higher energy for an absorber in a more positive valence state. For example, the edge shift amounts to 7 eV between Sm^{2+} in SmS and Sm^{3+} in SmP.[15] The structure of the main peak above the edge depends on the f occupancy and final-state effects. The L_3 spectra of trivalent lanthanide are characterized by a single peak above the edge. As shown in Fig. 1(a), La and rare earths in the T^*-phase samples all exhibit a single peak and the edges occur at the same position as in the corresponding trivalent oxides. Clearly, La, Sm, Eu, Gd, and Dy in the T^* compounds are trivalent.

The Tb L_3 spectrum of the $Tb_{0.9}$ sample differs from

other members of the T^* phases. Figure 1(b) displays the Tb L_3 spectra for T^*-phase $Tb_{0.9}$, T'-phase $Nd_{1.8}Tb_{0.2}CuO_4$, and Tb_4O_7. The energy scale is common for all three samples with the origin set at the half-height point of Tb_4O_7. It is known that $4f$ and valence-band hybridization may occur in Tb compounds; for example, Tb in TbO_2 has an f occupancy of 0.3 and cannot be strictly described as Tb^{4+}.[16] Tb $4f-O\,2p$ hybridization may also occur in the T^* compounds. Nevertheless, we will use the term Tb^{4+} or tetravalency for simplicity in our discussion, but with the understanding that it has a similar meaning as Tb valence in TbO_2. The Tb in $Nd_{1.8}Tb_{0.2}CuO_4$ shows a single-peak white line that is characteristic of Tb^{3+}. Above the edge, Tb_4O_7 exhibits two peaks of about equal amplitude separated by 8.6 eV. The low-energy peak is due to Tb^{3+} with a small contribution from Tb^{4+}, while the high-energy peak is due to Tb^{4+}. Their relative intensity is consistent with about equal amounts of Tb^{3+} and Tb^{4+} in Tb_4O_7. The main peak for the $Tb_{0.9}$ sample is followed by a shoulder at the same energy as that of the Tb^{4+} peak in Tb_4O_7. Since the Tb local environment in the T^* structure is similar to that in the T' structure (see below), this shoulder cannot be of structural origin judging from the spectrum of $Nd_{1.8}Tb_{0.2}CuO_4$. We attribute the shoulder to Tb^{4+} contributions in the T^*-phase $La_{0.9}Tb_{0.9}Sr_{0.2}CuO_4$ sample. The L_3 XANES data cannot distinguish whether the Tb^{4+} contribution is from isolated Tb^{4+} ions (among Tb^{3+}) or from mostly trivalent ions with some Tb^{4+} character. The Tb, La, and Sr EXAFS data (see below) suggest structural distortion in $La_{0.9}Tb_{0.9}Sr_{0.2}CuO_4$ as compared to other $R_{0.9}$ members. The structural distortion favors the existence of Tb^{4+} ions as opposed to the mostly trivalent ions with some Tb^{4+} character. We conclude that the $Tb_{0.9}$ compound contains both Tb^{4+} and Tb^{3+} ions.

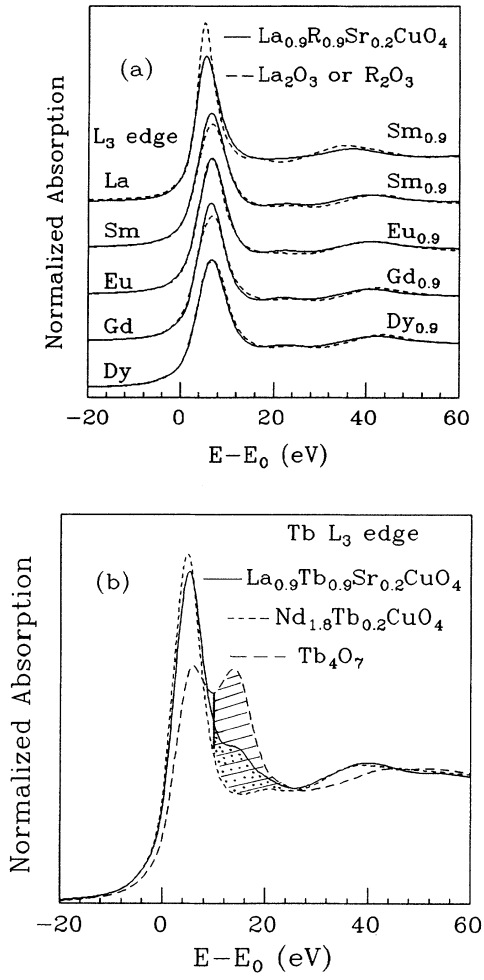

FIG. 1. (a) La and rare-earth L_3-edge XANES spectra of T^*-phase $La_{0.9}R_{0.9}Sr_{0.2}CuO_4$ (solid line) compared to those of oxides (dashed lines). (b) Tb L_3 spectra; the area of the shaded regions are used to estimate the amount of Tb^{4+} (see text).

The amount of Tb^{4+} is crudely estimated to be 20% of the total Tb ions as follows. Since the high-energy peak in the XANES spectrum arises from localized *f ground states,* [16] its intensity is insensitive to the specific crystal structure and is not significantly affected by the core-hole-induced final-state effects (this does not apply to the low-energy peak). The peak intensity thus provides a measure of the number of Tb^{4+} ions. In addition, the line shape of the main Tb^{3+} peak in the T^* sample is expected to be similar to that in $Nd_{1.8}Tb_{0.2}CuO_4$. The amount of Tb^{4+} is then estimated from the ratio between the area of the dot-shaded region and the line-shaded region [Fig. 1(b)], and bear in mind that the latter is due to about 50% Tb^{4+}. Ideally, one should decompose the spectrum into subspectra of Tb^{3+} and Tb^{4+} and compare their intensity; but the above estimate is sufficient for our purpose.

For the 160-bar oxygen-annealed $Tb_{0.9}$ sample, the shoulder at 14 eV is slightly stronger (not shown), suggesting a small increase in the Tb^{4+} percentage after oxygenation. We note that the Tb^{4+} observed here cannot be due to impurity phases that are not detectable in x-ray powder diffraction. We have also observed Pr^{4+} in a T^*-phase $Pr_{1.6}Sr_{0.4}CuO_4$ sample.

Having determined the valence of La and rare earths, we now turn to their site locations in the T^* phases. First, we identify a spectral feature in relevant structures. Figure 2(a) presents La and rare-earth L_3 XANES data for samples with T' structure. We draw attention to the peak labeled A at $\sim$20 eV. Feature A is present for Nd in Nd_2CuO_4, Gd in Gd_2CuO_4, and in particular La in T'-phase $Gd_{1.9}La_{0.1}CuO_4$. In addition, feature A is observed in the La spectra of T'-phase $Nd_{0.2}La_{0.2}CuO_4$ and $Nd_{1.5}La_{0.5}CuO_4$. Feature A also exists in the L_3 spectra of other members of T'-phase R_2CuO_4 (see Fig. 3).

Figure 2(b) displays the L_3 data for T-phase compounds. Feature A is completely absent in the spectra of La in both $La_{1.85}Sr_{0.15}CuO_4$ and $La_{1.4}Sm_{0.4}Sr_{0.2}CuO_4$. There is a weak residue of feature A in the Sm spectrum of $La_{1.4}Sm_{0.4}Sr_{0.2}CuO_4$. This residue is very likely to come from a T^* impurity phase, since about 5% T^*

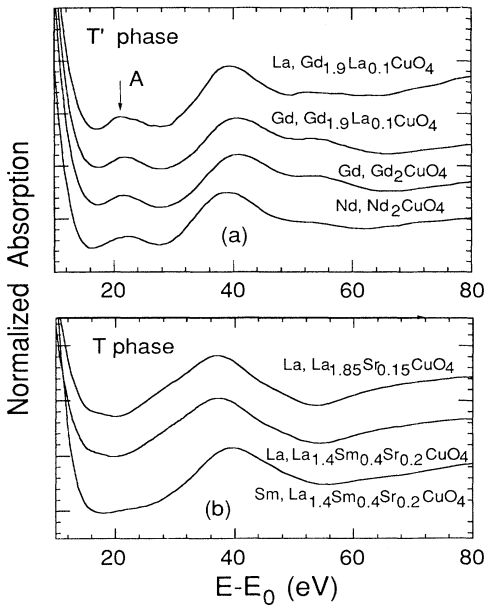

FIG. 2. La and rare-earth L_3 XANES data of (a) T'-phase and (b) T-phase samples. The element preceding the sample formula indicates the absorber. Feature A is present for La and rare earths in the T' structure, but is absent in the T structure. A weak residue of feature A in the Sm spectrum may arise from a T^*-phase impurity (see text).

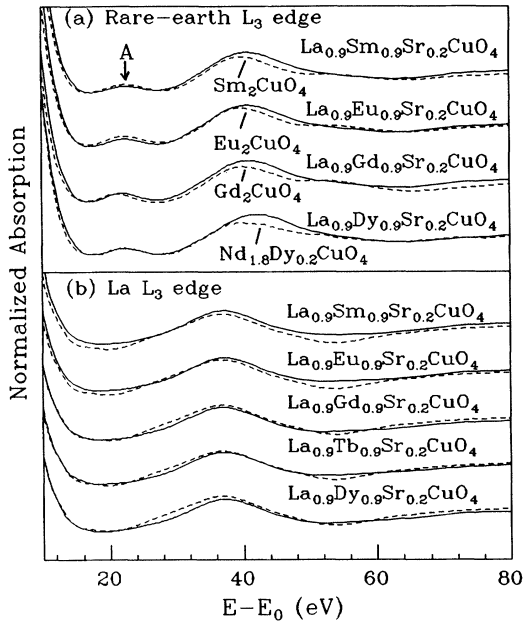

FIG. 3. (a) Rare-earth L_3 XANES spectra, comparing T^*-phase $La_{0.9}R_{0.9}Sr_{0.2}CuO_4$ (R = Sm, Eu, Gd, and Dy) with T'-phase R_2CuO_4. Note that feature A is common in the two structures. (b) La L_3 XANES spectra, comparing T^*-phase $La_{0.9}R_{0.9}Sr_{0.9}CuO_4$ (solid line) with the T-phase $La_{1.85}Sr_{0.15}CuO_4$ (dashed line). In both (a) and (b), E_0 is set at the half-height point of each absorption edge.

phase was detected in the x-ray-diffraction spectrum and Sm in the T^* structure exhibits feature A (see below). Feature A is also absent in the rare-earth L_3 data of other T-phase materials, for example, Gd in $La_{1.9}Gd_{0.1}CuO_4$ and $GdNaTiO_4$ and Pr in $PrSrCuO_4$. In summary, in the considerable number of the compounds we have measured, we always observe feature A in the L_3 spectra of La and trivalent rare earths in the T' structure, but not in the T structure.

Figure 3(a) shows the rare-earth L_3 spectra of T^*-phase $La_{0.9}R_{0.9}Sr_{0.2}CuO_4$ (solid line) and T'-phase R_2CuO_4 samples (dashed lines) for R = Sm, Eu, Gd, and Dy. Since the synthesis of T'-phase Dy_2CuO_4 requires high pressure,[17] we have made a $Nd_{1.8}Dy_{0.2}CuO_4$ sample to obtain a Dy site with T'-type local environment. Feature A is clearly present for Sm, Eu, Gd, and Dy in both T^* and T' structures with similar peak position and nearly identical peak intensity. We have also measured the Sm and Dy L_3 spectra for the 160-bar oxygenated $Sm_{0.9}$ and $Dy_{0.9}$ samples, respectively (not shown); feature A remains the same as in the as-prepared samples. Figure 3(b) exhibits the La L_3 spectra of T^*-phase $La_{0.9}R_{0.9}Sr_{0.2}CuO_4$ for R = Sm, Eu, Gd, Tb, and Dy together with that of the T-phase $La_{1.85}Sr_{0.15}CuO_4$ (dashed line). Looking at 20 eV, we find that feature A is essentially absent in all these T^* samples.

Now let us consider jointly the following facts. (1) Feature A is present for La and other trivalent rare earths in the T' structure, but is absent in the T structure (Fig. 2); (2) in the T^* structure, the M and M' site are locally similar to the lanthanide sites in the T and T' structures, respectively; and (3) Sm, Eu, Gd, and Dy in the T^* sample exhibit feature A with a similar intensity as that seen in the T' structure, and La shows a nearly vanishing feature A. These results clearly demonstrate that in T^*-phase $La_{0.9}R_{0.9}Sr_{0.2}CuO_4$, Sm, Eu, Gd, and Dy ions enter predominantly the M' site and the majority of La ions enter the M site. The similarity between the La spectra of the $Tb_{0.9}$ and other T^* samples [Fig. 3(b)] indicates that Tb and La also selectively enter the M' and M sites, respectively.

Because of the strong M-site preference of Sr,[9,10] a small amount of La has to occupy the M' site for the particular $La_{0.9}R_{0.9}Sr_{0.2}CuO_4$ composition; i.e., about one-ninth of the La ions enter the M' site in the case of a perfect cation ordering. La at the M' site should show a feature A. The XANES spectra in Fig. 3(b) are averaged over all La ions at both the M and M' sites. The feature A contributed from the M'-site La ions is not obvious as shown in Fig. 3(b). However, on an enlarged scale it becomes clear that the valley in the La spectra for the T^* samples is not quite as deep as that of $La_{1.85}Sr_{0.15}CuO_4$. This is consistent with the picture that a small fraction of La is at the M' site in $La_{0.9}R_{0.9}Sr_{0.2}CuO_4$.

Again, Tb in $Nd_{1.8}Tb_{0.2}CuO_4$ shows feature A as other trivalent lanthanide ions do in a T' local environment [Fig. 1(b)]. The change in the slope at about 19 eV in the spectrum of T^*-phase $La_{0.9}Tb_{0.9}Sr_{0.2}CuO_4$ [Fig. 1(b)] is suggestive of a feature A overlapping with the Tb^{4+} peak (shoulder). Thus the data are consistent with Tb^{3+} ions

occupying the M' site in this T^* sample. For tetravalent ions such as Ce, Th, and Tb, eightfold oxygen coordination is common, while ninefold coordination is rare. In the T^* structure, Tb^{4+} is expected to prefer strongly the M' site, which is coordinated by eight oxygens. In summary, the Tb site selectivity is in complete accordance with the La L_3 XANES data discussed above.

Our conclusion about the La and rare-earth site preference in the T^* compounds does not rely on the detailed interpretation of the physical origin of feature A, since the spectra of the T^* samples are compared with those of the closely related T and T' materials. It is, however, of fundamental interest to consider possible physical processes which give rise to feature A. Two likely possibilities are multiple scattering by the oxygen near neighbors and multielectron excitation. Backscattering by the cation neighbors is readily ruled out, since the cation configuration is essentially the same in the T and T' structures and feature A is absent in the former. In addition, A is present for Sm, Eu, and Gd, but is absent for La in the T^* structure, suggesting that the occurrence of feature A is determined by the oxygen neighbors.

To consider the possibility of multiple scattering, we have examined the scattering paths associated with feature A in real space for Gd_2CuO_4 as follows. First, the Fourier transform is obtained for the EXAFS function including feature A. Then parts of the Fourier-transform spectrum are selectively transformed back to k space (k is the photoelectron wave vector), the feature-A region of which is shown in Fig. 4. Clearly, the main intensity of feature A is associated with the 3.9–4.7-Å region in the Fourier-transform spectrum. The scattering paths are twice this value plus a phase-shift correction, which falls in the 9–12-Å range. Among a number of paths that are compatible with this range we single out the Gd-O-Gd-O'-Gd path, where O and O' are two oxygen atoms forming the body diagonal of the oxygen cage surrounding the Gd absorber. The O, Gd, and O' atoms are nearly collinear. The forward scattering by Gd can have an enhancement effect (shadowing) on the backscattered wave from O that is traveling toward O'. Thus the Gd-O-Gd-O'-Gd scattering can be significantly enhanced.

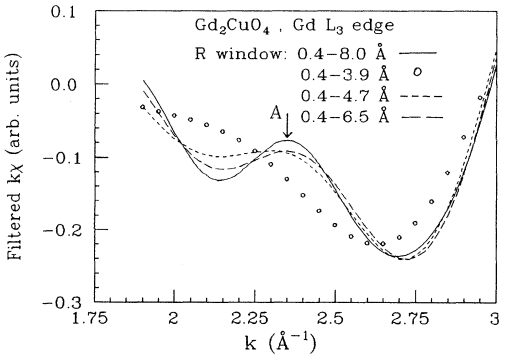

FIG. 4. Fourier-transform filtered Gd L_3 EXAFS function (multiplied by k) for Gd_2CuO_4. For clarity, data are shown only in the region where feature A appears. The R window indicated is the range for inverse transform from real to k space.

The position of feature A is remarkably insensitive to the type of absorber. It persistently appears at 16 eV above the white-line peak. If the photoabsorption is accompanied by a valence electron excitation, the photoelectron will have an energy smaller than in single-electron excitation by an amount equal to the excitation energy ΔE. For these events the fine structure will appear at a higher photon energy by ΔE. In particular, the white line shifted to a higher energy by ΔE could appear as feature A. If feature A is due to the shifted white line, its intensity should be proportional to the white-line intensity. We found that the feature-A–to–white-line intensity ratios are about the same for the L_3 and L_2 spectra of Nd_2CuO_4. The multielectron excitation picture is compatible with this finding.

To look into the possibility of a dipole-forbidden $2p$-$5p$ transition, we have compared the Nd L_1 and L_3 spectra of Nd_2CuO_4 on a common energy scale by lining up the EXAFS oscillations as suggested by Lytle and Greegor.[18] We found that feature A appears at ~ 5 eV above the L_1 main peak which is due to transitions from the $2s$ to the p-like final states. This finding argues against a $2p$-$5p$ transition as the origin of feature A, since such a transition is expected to peak at the L_1 main peak.

Based on above considerations, we believe that feature A is likely to arise from multiple scattering by the oxygen near neighbors or from a multielectron excitation event.

B. EXAFS data

The EXAFS spectrum is determined by the type and number of near neighbors and their distances to the absorber. By analyzing the EXAFS data measured at the La and rare-earth absorption edges, the local environment around La and R ions can be determined. Such an analysis also led us to the conclusion that La and rare earths are ordered in T^*-phase $La_{0.9}R_{0.9}Sr_{0.2}CuO_4$. The M site is coordinated with nine oxygens, one at ~ 2.3 Å, four at ~ 2.6 Å, and four at ~ 2.7 Å. On the other hand, the M' site is coordinated with eight oxygens, four at ~ 2.3 Å and four at ~ 2.6 Å. Such coordinations for the M and M' sites are sufficiently different to allow an independent determination of the site location of the rare-earth ions by studying the oxygen neighbor contribution to the EXAFS function.

Figure 5 displays the Fourier transforms of the Sm, Gd, Tb, and Dy L_3 EXAFS function in T^*-phase $La_{0.9}R_{0.9}Sr_{0.2}CuO_4$. The overall spectral features of these samples are similar except that the Tb spectrum is somewhat different from others. To quantify the oxygen coordination configuration, we have analyzed the oxygen contributions by nonlinear least-square fitting. Standards for the EXAFS amplitude and phase-shift values were extracted from $LaSmSrCu_2O_6$ and $LaGdSrCu_2O_6$ for Sm-O and Gd-O pairs, respectively. $LaSmSrCu_2O_6$ and $LaGdSrCu_2O_6$ have $La_2SrCu_2O_6$-type tetragonal structure.[19] Sm and Gd occupy the site between the double CuO_2 layers and have eight oxygen neighbors at a

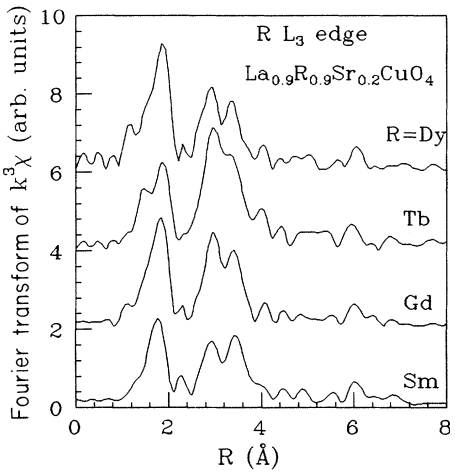

FIG. 5. Fourier-transform magnitudes of rare-earth L_3 EXAFS data for $La_{0.9}R_{0.9}Sr_{0.2}CuO_4$ (R = Sm, Gd, Tb, and Dy).

single distance.[20] The Sm EXAFS data for both $La_{0.9}Sm_{0.9}Sr_{0.2}CuO_4$ and Sm_2CuO_4 were fitted using the Sm-O reference. The Gd data for $La_{0.9}Gd_{0.9}Sr_{0.2}CuO_4$ and Gd_2CuO_4 and Tb data for $La_{0.9}Tb_{0.9}Sr_{0.2}CuO_4$ were fitted using the Gd-O reference. The initial fitting assumed that the rare-earth ions are taking the M' position with the coordination number fixed. This led to a well-defined distance for the four nearest oxygen neighbors O(3). The distance for the other four oxygen atoms O(1) is less well defined and is sensitive to the energy shift. By adjusting the energy shift, good agreement is obtained between the data and fit. Once the energy shift and distances are fixed, the coordination numbers (N) were also varied, and the resulting value remained close to 4.0 for both O(3) and O(1) in the Sm samples, but a deviation from 4.0 for O(1) occurred for the Gd and Tb samples. This deviation is probably due to the correlation between N and the pair disorder parameter ($\Delta\sigma^2$). Considering the behavior of N for O(3), N values were fixed to 4.0 for both O(1) and O(3) atoms in the final fitting. The Sm-O and Gd-O distances in $LaSmSrCu_2O_6$, and $LaGdSrCu_20_6$, respectively, are not known to high precision. However, their values are close to 2.50 Å, judging from the Nd-O distance of 2.511 Å in $LaNdSrCu_2O_6$.[21] The Sm-O and Gd-O distances were adjusted to give a M'-O distance that matches the values determined by neutron diffraction on $La_{0.9}Sm_{0.9}Sr_{0.2}CuO_4$ and $La_{0.9}Gd_{0.9}Sr_{0.2}CuO_4$.

Structural parameters obtained from the fitting are listed in Table I. The R-O(3) distance, coordination number, and disorder parameter appear to be well defined in the fitting. We estimate the relative uncertainty in N for O(3) to be ~10%. This gives the uncertainty of the site determination based on the EXAFS fitting, since N(O(3)) is affected by the same percentage of any site disorder between M' and M sites. Within an uncertainty of 10%, our EXAFS analysis results indicate that Sm, Gd, and Tb occupy only the M' site in the corresponding $La_{0.9}R_{0.9}Sr_{0.2}CuO_4$ samples. By fixing the R-O(3) distance to that determined by neutron diffraction, the R-O(1) distance obtained in our fit also agreed with the neutron data, which attests to the validity of the fitting. As shown in Table I, the pair disorder parameters $\Delta\sigma^2$ for the Sm-O(3) and Sm-O(1) pairs are similar in $Sm_{0.9}$, while in $Gd_{0.9}$ and $Tb_{0.9}$ samples, the R-O(1) pair is more disordered than R-O(3). Similarly, the pairs with the longer bond length [R-O(1)] in Gd_2CuO_4 are more disordered.

TABLE I. Parameters for R-O bonds in T^*-phase $La_{0.9}R_{0.9}Sr_{0.2}CuO_4$ and R_2CuO_4 obtained from fitting the rare-earth L_3 EXAFS spectra. The EXAFS phase and amplitude parameters were extracted from $LaSmSrCu_2O_6$ and $LaGdSrCu_2O_6$, and the Sm-O and Gd-O distances were assumed to be 2.47 and 2.45 Å, respectively. The mean-squared variation of bond lengths $\Delta\sigma^2$ is relative to that in the corresponding reference compound. Numbers in parentheses are uncertainty in the last digit(s).

Samples	Pair	R (Å)	N	$\Delta\sigma^2$ (Å^2)
Sm_2CuO_4	Sm-O(1)	2.70(4)	4	0.001(6)
	Sm-O(2)	2.34(2)	4	−0.006(2)
$La_{0.9}Sm_{0.9}Sr_{0.2}CuO_4$	Sm-O(1)	2.55(3)	4	0.003(5)
	Sm-O(3)	2.34(2)	4	−0.004(2)
Gd_2CuO_4	Gd-O(1)	2.63(13)	4	0.034(26)
	Gd-O(2)	2.33(2)	4	−0.005(1)
$La_{0.9}Gd_{0.9}Sr_{0.2}CuO_4$	Gd-O(1)	2.49(5)	4	0.018(16)
	Gd-O(3)	2.31(2)	4	−0.003(1)
$La_{0.9}Tb_{0.9}Sr_{0.2}CuO_4$	Tb-O(1)	2.47(7)	4	0.021(29)
	Tb-O(3)	2.32(2)	4	0.001(4)

Knowing that the rare-earth ions enter only the M' site, La can occupy the M site and the remaining M' site in T^*-phase $La_{0.9}R_{0.9}Sr_{0.2}CuO_4$. The Fourier transform of La EXAFS spectra is shown in Fig. 6 for R = Sm, Gd, Tb, and Dy. The spectrum for R = Eu is identical to those of Sm and Gd samples and is omitted for clarity. The oxygen peaks (1.0–3.0 Å) are nearly identical for R = Sm, Gd, and Dy, indicating a nearly identical La local environment in these samples. The $Tb_{0.9}$ sample shows a small but clear difference from others in the oxygen peak, suggestive of distortion in the oxygen neighbors. The M' site is off center in the oxygen cage. Tb^{4+} ions may prefer a more centered position and cause distortion in the nearby oxygen positions. Trivalent ions with a small Tb^{4+} character are less likely to cause significant distortion. In this sense the distortion suggested by the Tb, La, and Sr (Fig. 7) EXAFS data favors the existence of Tb^{4+} ions in the Tb T^* compound, as was referred to in the discussion of the Tb XANES data.

Figure 7 presents the Sr K-edge EXAFS data for Sm, Eu, Gd, and Tb T^* materials. The spectra of Sm, Eu, and Tb samples are compared with that of the Gd sample (dashed line). The spectra, including detailed features,

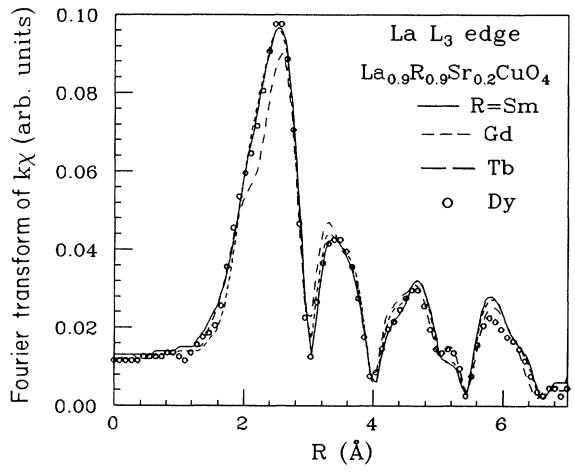

FIG. 6. Fourier-transform magnitude of La L_3 EXAFS for T^*-phase $La_{0.9}R_{0.9}Sr_{0.2}CuO_4$ (R =Sm, Gd, Tb, and Dy).

for the Sm, Eu, and Gd samples are surprisingly similar, suggesting identical Sr local environments. Again, there is a small difference in the Tb sample as compared to others.

The rare-earth L_3-edge, La L_3-edge, and Sr K-edge EXAFS results can be summarized as follows. From fitting the rare-earth EXAFS data, nearly exclusive M'-site selectivity by the rare-earth ions is revealed. The extreme insensitivity of La and Sr EXAFS spectra to rare-earth ion variation in the $La_{0.9}R_{0.9}Sr_{0.2}CuO_4$ series shows that the degree of the cation ordering is about the same for R =Sm through Dy.

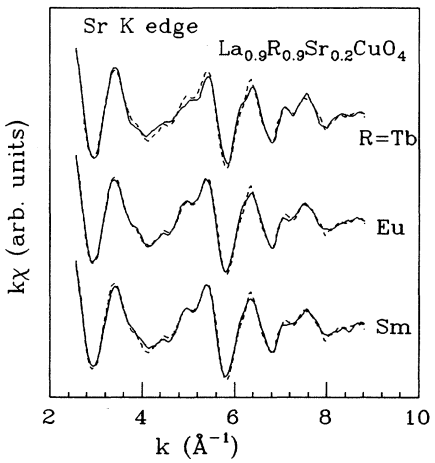

FIG. 7. Sr K-edge EXAFS data for T^*-phase $La_{0.9}R_{0.9}Sr_{0.2}CuO_4$ with R =Sm, Eu, Gd, and Tb. The spectrum for the Gd sample is plotted as the dashed line with others (solid line).

IV. Cu XANES RESULTS

The CuO_2 plane is the main conduction path in the cuprate superconductors. The electronic states of primary importance are the Cu 3d and O 2p states. Oxygen K-edge x-ray-absorption and electron-energy-loss spectroscopy (EELS) studies have provided direct evidence for holes of O 2p character in p-type $La_{2-x}Sr_xCuO_4$ and $YB_2Cu_3O_7$ superconductors (e.g., Refs. 23 and 24), and Cu K-edge studies have elucidated the nature of electron doping in n-type superconductors.[25,26] Here we present Cu K-edge XANES data for the superconducting and nonsuperconducting T^*-phase $La_{0.9}R_{0.9}Sr_{0.2}CuO_4$ compounds.

A common energy scale is used for the Cu K-edge data, and the origin is set at the inflection point of the copper-metal spectrum. All spectra presented here are normal-

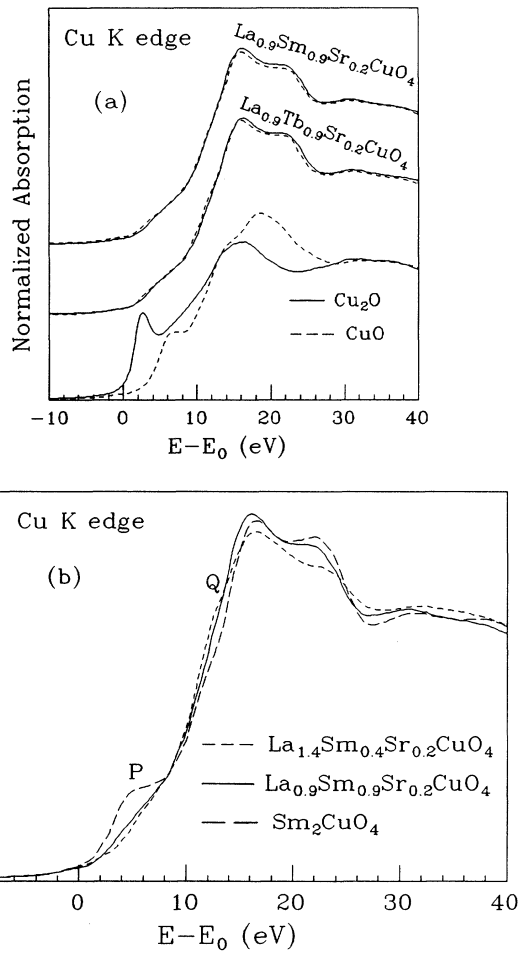

FIG. 8. Cu K-edge XANES spectra (E_0 is set at the inflection point of the copper-metal spectrum). (a) As-prepared (solid line) and 160-bar oxygenated (dashed line) T^*-phase $La_{0.9}Sm_{0.9}Sr_{0.2}CuO_4$ and $La_{0.9}Tb_{0.9}Sr_{0.2}CuO_4$ along with those of CuO and Cu_2O. (b) Comparison among the T-, T^*-, and T'-structured $La_{1.4}Sm_{0.4}Sr_{0.2}CuO_4$, $La_{0.9}Sm_{0.9}Sr_{0.2}CuO_4$, and Sm_2CuO_4, respectively. Features P and Q are discussed in the text.

ized to the edge jump. Figure 8(a) shows the Cu XANES spectra for as-prepared and 160-bar oxygen-treated T^*-phase $La_{0.9}Sm_{0.9}Sr_{0.2}CuO_4$ and $La_{0.9}Tb_{0.9}Sr_{0.2}CuO_4$. The oxygenated Sm sample is superconducting, but the as-prepared one is not. Neither the as-prepared nor oxygenated Tb sample is superconducting. We note that the oxygen-treated samples were stored in liquid nitrogen to prevent oxygen diffusion. The main absorption edge lines up with those of CuO and Sm_2CuO_4 [see also Fig. 8(b)], consistent with divalent copper in the T^* compounds. The spectra for as-prepared and oxygenated samples are essentially identical, and the difference between the Sm and Tb samples is also minimal. These results demonstrate that the occurrence of superconductivity in the T^* material is not accompanied by any appreciable change of the copper electronic states observable in the Cu K-edge spectra.

Although p-type cuprate superconductors are frequently described to have a copper valence greater than 2, the Cu ground state has little $3d^8$ character because of large on-site d-d Coulomb repulsion. The doping is largely associated with O $2p$ states, and the Cu states are affected to a lesser extent. In the present case of T^*-phase compounds, we observe essentially no difference in the Cu K-edge spectra between the superconducting and nonsuperconducting samples. We anticipate hole doping to take place on the oxygen states.

Figure 8(b) compares the Cu XANES data among $La_{0.9}Sm_{0.9}Sr_{0.2}CuO_4$, $La_{1.4}Sm_{0.4}Sr_{0.2}CuO_4$, and Sm_2CuO_4, which are of T^*, T, and T' structures, respectively. All three show a main edge at about the same energy. Of interest here are features P and Q. Both P and Q arise from $2s$-$4p_\pi$ transitions for copper in a $3d^9$ ground state; but for P the transition is accompanied by a ligand-to-metal charge transfer.[26–28] P is strongest in Sm_2CuO_4 in which Cu is coordinated with only four in-plane oxygens. The intensity of P is drastically reduced by the addition of an apical oxygen in T^*-phase $La_{0.9}Sm_{0.9}Sr_{0.2}CuO_4$ and is further reduced in T-phase $La_{1.4}Sm_{0.4}Sr_{0.2}CuO_4$ in which two apical oxygens are present. In correspondence to the reduction in P, the intensity of Q increases. This shows that the apical oxygen very effectively inhibits the ligand-to-copper charge transfer. In other words, even with an attractive potential created by the core hole, the ability for Cu to accept an electron is much reduced by the apical oxygen. This is probably why the T and T^* structures cannot be doped with electrons.

V. DISCUSSION

A. Superconductivity and rare-earth concentration

By studying the La and rare-earth L_3 XANES and EXAFS data, we have shown that the La and R ions enter the M and M' sites, respectively, in an ordered way in T^*-phase $La_{0.9}R_{0.9}Sr_{0.2}CuO_4$ for R = Sm through Dy. The degree of the observed cation ordering is nearly perfect and is similar for Sm, Eu, Gd, Tb, and Dy members of the family. Our results are in agreement with x-ray and neutron-diffraction studies in similar Gd and Sm T^* materials.[9,22] A number of properties of T^*-phase compounds can be better understood based on the cation ordering; for example, the narrow range of phase homogeneity of the T^* phase is likely due to the tendency of cation site ordering and competition between the T and T' structures.[10,29]

Here we consider the relationship between the cation ordering and superconducting properties of the T^* materials. In Fig. 9 we have plotted the T_c data of Fisk *et al.*[6] as a function of the rare-earth concentration x for 150-bar oxygenated T^*-phase $La_{1.8-x}R_xSr_{0.2}CuO_4$. Also plotted are the T_c data for rare-earth substituted T-phase $La_{2-y}Sr_yCuO_4$.[30,31] The T_c values all refer to the onset of diamagnetism. For T^* compounds, superconductivity occurs in a narrow region centered near $x = 0.9$–1.0. This region for the Sm T^* sample is relatively broad, but the Meissner data peak in a narrower region near $x = 0.9$.[6] The phase boundaries between the T, T^*, and T' phases are only schematic; the details depend on the rare-earth combination and, to a lesser extent, on the preparation conditions. In T-phase $La_{2-y}Sr_yCuO_4$, rare-earth substitution reduces T_c substantially without affecting the overall structural symmetry. The degree of T_c suppression clearly correlates with the ionic radius; namely, the smaller ions are more effective in suppressing T_c.[30,32] The mechanism responsible for the T_c suppression has been under considerable discussion.[30–33] Based on a fairly convincing argument, magnetic exchange interactions and volume effects have been ruled out as the principal mechanisms. There appear to be two remaining possibilities, *local structural disorder* and *oxygen vacancies*. Because of the size mismatch between the (La Sr) and rare-earth ions, local strain may be produced upon substitution. In addition, the oxygen coordination configuration in the T structure is quite uncommon for rare-earth ions other than La. The T' structure of

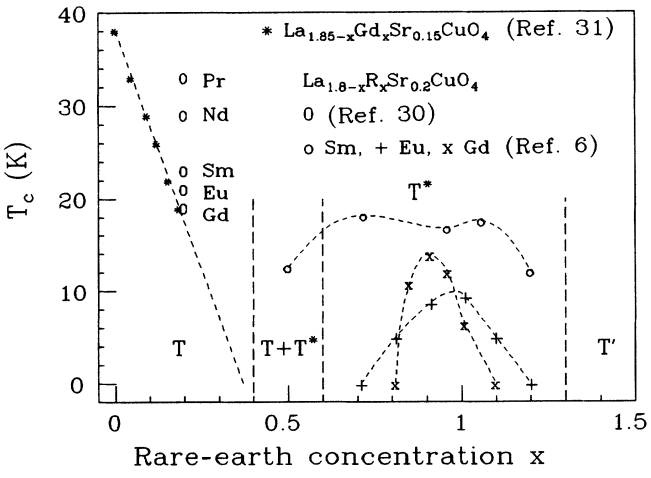

FIG. 9. Superconducting transition temperature T_c (the onset of diamagnetism) as a function of rare-earth concentration in T^*-phase $La_{1.8-x}R_xSr_{0.2}CuO_4$ (from Ref. 6) and in T-phase $La_{1.85-x}Gd_xSr_{0.15}CuO_4$ (Ref. 31) and $La_{1.8-x}R_xSr_{0.2}CuO_4$ (R = Pr, Nd, Sm, Eu, and Gd) (Ref. 30).

R_2CuO_4 for $R=Pr,Nd,\ldots,Gd$ and the M' site preference for rare earths in the T^* structure suggests that the rare-earth ions prefer a T'-type oxygen configuration. It is likely that rare earths substituting in $La_{1.8}Sr_{0.2}CuO_4$ cause distortions in the local oxygen environment, which can affect the CuO_2 plane. *Local structural disorder* as used in this paper hereafter includes both strain due to size mismatch and possible distortion in the oxygen configuration. Since T_c generally depends on the hole concentration, T_c may be reduced if the rare-earth substitution creates oxygen vacancies that reduce the hole concentration.

The sensitiveness of T_c suppression to the size of the rare-earth ions strongly suggests that the local structural disorder is the main factor that reduces T_c. Clearly, this mechanism is also operational in the T^*-phase materials. In T^*-phase $La_{2-x-y}R_xSr_yCuO_4$, the La (Sr) and R ions tend to enter in an orderly fashion the M and M' sites, respectively. Thus structural disorder caused by a random distribution of La (Sr) and R ions is eliminated at $x=1.0$ in the case of a perfect ordering. Correspondingly, as shown in Fig. 9, T_c is maximum near $x=1.0$. In fact, the highest-T_c value (37 K) achieved in the 3-kbar oxygen-annealed Sm T^* sample[5] is close to that of $La_{1.85}Sr_{0.15}CuO_4$. Once the rare-earth concentration deviates from this optimum value, a mixture of La (Sr) and R ions starts to occupy one of the M and M' sites. Such a mixture at one site resembles the rare-earth substitution in $La_{2-y}Sr_yCuO_4$ and suppresses T_c. Again, T_c suppression depends on the size of the rare-earth ions; i.e., the smallest Gd ion suppresses T_c more effectively than the Eu and Sm ions (Fig. 9). The decrease of T_c for $x\leq 1.0$ in Fig. 9 shows a mixture of La and rare earths at the M' site suppresses T_c as effectively as at the M site. T_c in $Nd_{1.85}Ce_{0.15}CuO_4$ is suppressed by La substitution,[13,34] but is hardly affected by Sm substitution.[34] In this case there is a size mismatch for both Nd-La and Nd-Sm combinations as evidenced by the change in lattice parameters upon substitution. However, there is a disparity in the local-oxygen-environment preference for Nd and La, but not for Nd and Sm. Thus the disparity in the local-oxygen- environment preference also plays an important role in the suppression of T_c.

Since T^*-phase superconductors are high-pressure oxygenated, the decrease of T_c for a rare-earth concentration deviating from the optimum value is not likely to be due to more oxygen vacancies in such samples. Thus the local structural disorder caused by mismatch of ionic radii and the disparity in the local-environment preference appears to be the most plausible mechanism for the suppression of T_c in the rare-earth-substituted systems.

B. Lack of superconductivity

In this section we discuss possible reasons why the Tb and Dy T^* compounds are not superconducting. The necessity of high-pressure oxygen annealing to produce superconductivity in the Sm, Eu, and Gd T^* phases suggests the existence of oxygen vacancies in samples prepared under ambient pressure. A neutron-diffraction study indicated an oxygen content of 3.87 for as-prepared $La_{0.9}Sm_{0.9}Sr_{0.2}CuO_4$ which increases to essentially 4.0 after oxygenation at 3 kbar.[22] The oxygen vacancies were found to be at the facial site O(3) in the T'-like layer. The Eu and Gd compounds are expected to behave similarly. From our thermogravimetric analysis (TGA), the oxygen content of our as-prepared $La_{0.9}Tb_{0.9}Sr_{0.2}CuO_4$ and $La_{0.9}Dy_{0.9}Sr_{0.2}CuO_4$ samples was found to be 3.99 ± 0.02 and 3.91 ± 0.02, respectively. The oxygen content in the Tb T^* sample remains essentially unchanged after 160-bar oxygen annealing. Refinement of neutron-diffraction data on an as-prepared $La_{1.0}Tb_{0.8}Sr_{0.2}CuO_4$ sample revealed an oxygen content of 3.94 ± 0.03.[35] These data suggest that the amount of oxygen deficiency in the Tb T^* compound is less than that in the Sm and Dy analogs. The lack of superconductivity in Tb T^*-phase samples may be attributed to the presence of a significant amount of Tb^{4+} which reduces the hole concentration. The presence of Tb^{4+} is probably also responsible for the higher oxygen content than in other members of the T^* compounds, presumably by preventing the formation of oxygen vacancies at the O(3) site.

As our TGA data indicated, the oxygen content of the $La_{0.9}Dy_{0.9}Sr_{0.2}CuO_4$ sample became 3.92 ± 0.02 after the 160-bar oxygenation as compared to 3.91 ± 0.02 before the treatment. It appears that the high-pressure oxygenation does not fill in the oxygen vacancies and thus does not raise the hole concentration as in the Sm, Eu, and Gd analogs. Additionally, even if the hole concentration is appropriate, the observation of superconductivity would depend critically on the cation concentration. This can be visualized in Fig. 9, in which the superconducting region becomes progressively narrower as the rare earth gets smaller in T^*-phase $La_{1.8-x}R_xSr_{0.2}CuO_4$ (R = Sm, Eu, and Gd). Because of the large difference between the sizes of Dy and La (Sr) ions, any sizable random distribution of these ions at one type of site may prevent the material from being superconducting according to the mechanism of T_c suppression by increased local structural disorder discussed in the previous section.

ACKNOWLEDGMENTS

We wish to thank Dale Brewe for assistance in the experiments. Z.T. thanks Steve Heald and John Tranquada for stimulating discussions. The University of Connecticut group acknowledges the support from the U.S. Department of Energy, under Contract Nos. DE-AS05-80-ER10742 and DE-FG02-90ER45424. The x-ray-absorption experiments were carried out at Beam Line X-11 at the National Synchrotron Light Source (NSLS), and NSLS is supported by the Department of Energy under Contract No. DE-AC02-76CH00016. Work carried out at Los Alamos was supported by the Department of Energy.

*Present address: Building 480, Brookhaven National Laboratory, Upton, NY 11973.
[1]J. Akimitsu, S. Suzuki, M. Watanabe, and H. Sawa, Jpn. J. Appl. Phys. **27**, L1859 (1988).
[2]E. Takayama-Muramachi, Y. Matsui, Y. Uchida, F. Izumi, M. Onoda, and K. Kato, Jpn. J. Appl. Phys. **27**, L2283 (1988).
[3]Y. Tokura, A. Fujimori, H. Matsubara, H. Watabe, H. Ikeda, S. Okuda, and S. Tanaka, Phys. Rev. B **39**, 9704 (1989).
[4]S-W. Cheong, Z. Fisk, J. D. Thompson, and R. B. Schwarz, Physica C **159**, 407 (1989).
[5]M. F. Hundley, J. D. Thompson, S-W. Cheong, Z. Fisk, R. B. Schwarz, and J. E. Schirber, Phys. Rev. B **40**, 5251 (1989).
[6]Z. Fisk, S-W. Cheong, J. D. Thompson, M. F. Hundley, R. B. Schwarz, G. H. Kwei, and J. E. Schirber, Physica C **162-164**, 1681 (1989).
[7]H. Sawa, S. Suzuki, M. Watanabe, J. Akimitsu, H. Matsubara, H. Watabe, S. Uchida, K. Kokusho, H. Asano, F. Izumi, and E. Takayama-Muromachi, Nature **337**, 347 (1989).
[8]F. Izumi, E. Takayama-Muromachi, A. Fujimori, T. Kamiyama, H. Asano, I. Akimitsu, and H. Sawa, Physica C **158**, 440 (1989).
[9]G. H. Kwei, R. B. Von Dreele, S-W. Cheong, Z. Fisk, and J. D. Thompson, Phys. Rev. B **41**, 1889 (1990).
[10]Z. Tan, J. I. Budnick, W. Q. Chen, D. L. Brewe, S-W. Cheong, A. S. Cooper, and L. W. Rupp, Jr., Phys. Rev. B **42**, 4808 (1990).
[11]P. Lightfoot, S. Pei, J. D. Jorgensen, X-X. Tang, A. Manthiram, and J. B. Goodenough, Physica C **169**, 15 (1990).
[12]S-W. Cheong (unpublished).
[13]E. Wang, J-M. Tarascon, L. H. Greene, G. W. Hull, and W. R. Mckinnon, Phys. Rev. B **41**, 6582 (1990).
[14]A. Manthiram, X-X. Tang, and J. B. Goodenough, Phys. Rev. B **42**, 138 (1990).
[15]J. B. Boyce, R. M. Martin, and J. W. Allen, in *EXAFS and Near Edge Structure,* edited by A. Bianconi, L. Incoccia, and S. Stipcich (Springer-Verlag, New York, 1983), p. 187.
[16]H. Dexpert, R. C. Karnatak, J.-M Esteva, J. P. Connerade, M. Gasgnier, P. Caro, and L. Albert, Phys. Rev. B **36**, 1750 (1987).
[17]H. Okada, M. Takano, and Y. Takeda, Physica C **166**, 111 (1990).
[18]F. W. Lytle and R. B. Greegor, Appl. Phys. Lett. **56**, 192 (1990).
[19]N. Nguyen, L. Er-Rakho, C. Michel, J. Choisnet, and B. Raveau, Mater. Res. Bull. **15**, 891 (1980); V. Caignaert, N. Nguyen, and B. Raveau, *ibid.* **25**, 199 (1990).
[20]S-W. Cheong *et al.* (unpublished).
[21]R. Grasmeder amd M. T. Weller, J. Solid State Chem. **85**, 88 (1990).
[22]G. H. Kewi (unpublished).
[23]N. Nücker, J. Fink, J. C. Fuggle, P. J. Durham, and W. M. Temmerman, Phys. Rev. B **37**, 5158 (1988).
[24]P. Kuiper, G. Kruizinga, J. Ghijsen, M. Grioni, P. J. W. Weijs, F. M. F. de Groot, G. A. Sawatzky, H. Verweij, L. F. Feiner, and H. Petersen, Phys. Rev. B **38**, 6483 (1988).
[25]J. M. Tranquada, S. M. Heald, A. R. Moodenbaugh, G. Liang, and M. Croft, Nature **337**, 720 (1990).
[26]Z. Tan, J. I. Budnick, C. E. Bouldin, J. C. Woicik, S-W. Cheong, A. S. Cooper, G. P. Espinosa, and Z. Fisk, Phys. Rev. B **42**, 1037 (1990), and references cited therein.
[27]S. M. Heald, J. M. Tranquada, A. R. Moodenbaugh, and Y. Xu, Phys. Rev. B **38**, 761 (1988).
[28]N. Kosugi, Y. Tokura, H. Takagi, and S. Uchida, Phys. Rev. B **41**, 131 (1990).
[29]J. F. Bringley, S. S. Trail, and B. A. Scott, J. Solid State Chem. **86**, 310 (1990).
[30]J-M. Tarascon, L. H. Greene, W. K. Mckinnon, and G. W. Hull, Solid State Commun. **63**, 499 (1987).
[31]G. Xiao, M. Z. Cieplak, and C. L. Chien, Phys. Rev. B **40**, 4538 (1989).
[32]H. Takagi, S. Uchida, H. Eisaki, S. Tanaka, K. Kishio, K. Kitazawa, and K. Fueki, J. Appl. Phys. **63**, 4009 (1988).
[33]G. W. Crabtree, W. K. Kwok, A. Umezawa, L. Soderholm, L. Morss, and E. E. Alp, Phys. Rev. B **36**, 5258 (1987).
[34]K. Oh-Ishi, Y. Syono, M. Kikuchi, N. Kobayashi, and Y. Muto, Solid State Commun. **73**, 341 (1990).
[35]P. Bordet, S-W. Cheong, Z. Fisk, Th. Fournier, J. L. Hodeau, M. Marezio, A. Santoro, and A. Varela, Physica C **171**, 468 (1990).